Journal of Alloys and Compounds 788 (2019) 565–572

Contents lists available at ScienceDirect

Journal of Alloys and Compounds

journal homepage: http://www.elsevier.com/locate/jalcom

Stability and electrochemical performance of nanostructured $La_2CuO_{4+\delta}$ cathodes

L. dos Santos-Gómez [a], J.M. Porras-Vázquez [a], J. Hurtado [b], E.R. Losilla [a], D. Marrero-López [b, *]

[a] Universidad de Málaga, Departamento de Química Inorgánica, 29071, Málaga, Spain
[b] Universidad de Málaga, Departamento de Física Aplicada I, 29071, Málaga, Spain

ARTICLE INFO

Article history:
Received 20 December 2018
Received in revised form
18 February 2019
Accepted 21 February 2019
Available online 22 February 2019

Keywords:
Solid oxide fuel cells
Nanostructured electrodes
$La_2CuO_{4+\delta}$
$Ce_{0.9}Gd_{0.1}O_{2-\delta}$

ABSTRACT

$La_2CuO_{4+\delta}$ cathode layers are prepared by spray-pyrolysis deposition and their structural, microstructural and electrical properties are compared with those of submicrometric powders obtained from freeze-dried precursors. In order to improve the cathode performance, three different electrode architectures have been proposed: (i) powder cathodes obtained by conventional screen-printing and sintering, and cathodes deposited by spray-pyrolysis on: (ii) as-prepared electrolyte surfaces and (iii) porous electrolyte backbones. The cathode activity for the oxygen reduction reaction has been investigated as a function of the microstructure and the sintering temperature. The microstructural optimization of the cathodes and the low fabrication temperature minimize the instability problems between the electrolyte and the cathode materials, leading to polarization resistances as low as 0.14 Ω cm^2 at 600 °C.

1. Introduction

Solid Oxide Fuel Cells (SOFCs) and Solid Oxide Electrolyzer Cells (SOECs) are efficient and environmentally friendly technologies for power generation and storage [1,2]. However, the degradation problems associated with the high operating temperature of these devices, such as chemical reaction between the materials, surface phase segregations and delamination of the materials layers during thermal cycling, are the main obstacle for their widespread commercialization [3–5]. Different strategies have been explored to lower the SOFC operating temperature below 700 °C, including the development of alternative solid electrolytes to the commonly used $Zr_{0.84}Y_{0.16}O_{1.92}$ (YSZ) and the deposition of thin film electrolytes to reduce the ohmic resistance of the cell [6,7]. Hence, nowadays, the SOFC performance at low temperature is mainly limited by the cathode polarization resistance [8].

Numerous cathode materials with enhanced performance, compared to the conventional $La_{0.8}Sr_{0.2}MnO_{3-\delta}$, have been identified in the last few years, including $La_{0.8}Sr_{0.2}Fe_{0.8}Co_{0.2}O_{3-\delta}$, $Ba_{0.5}Sr_{0.5}Co_{0.8}Fe_{0.2}O_{3-\delta}$ (BSCF), $BaCo_{0.4}Fe_{0.4}Zr_{0.2}O_{3-\delta}$ and $LnBaCo_2O_{5+\delta}$ (Ln = Gd and Pr) [9–12]. However, these cobalt-based electrodes often suffer from several drawbacks, such as the high cost of cobalt, high thermal expansion coefficients and phase degradation in the case of BSCF [13,14]. Among other studied compounds, Ruddlesden-Popper phases, $Ln_2MO_{4+\delta}$ (Ln = La, Pr and Nd; M = Ni and Cu), are of particular interest due to their high mixed ionic and electronic conductivity, moderate thermal expansion coefficients and mechanically compatible with the electrolyte. In addition, cathode materials without alkaline-earth elements are less prone to surface carbonation and degradation [15–17].

In this family of compounds, lanthanum nickelates have received a great deal of attention because of their higher electronic conductivity [15,16,18]. However, one of the main drawbacks associated with these materials is the chemical reactivity with the electrolyte. For instance, Sayer et al. have reported reactivity between La_2NiO_4 and $Ce_{0.9}Gd_{0.1}O_{1.95}$ (CGO) above 800 °C, while Montenegro-Hernández et al. observed reactivity by transmission electron microscopy at only 700 °C, which is accompanied by an increase of the electrode polarization resistance over time, from 7 to 10 Ω cm^2 for 85 h at 750 °C [19–21]. Recently, Cetin et al. have also observed the decomposition of La_2NiO_4 in $Sm_{0.2}Ce_{0.8}O_2$-La_2NiO_4 composite cathodes [22].

It is well known that the reactivity between the electrolyte and electrode materials mainly depends on the fabrication method and

* Corresponding author. Dpto. de Física Aplicada I, Facultad de Ciencias, Campus de Teatinos, Universidad de Málaga, 29071, Málaga, Spain.
E-mail address: marrero@uma.es (D. Marrero-López).

https://doi.org/10.1016/j.jallcom.2019.02.237
0925-8388/

the sintering temperature. In general, electrode powders obtained by conventional preparation methods require of high sintering temperatures in order to achieve sufficient adherence between the electrode and the electrolyte, and consequently, it is difficult to avoid the reactivity between the materials. On the other hand, the electrode performance is not only determined by the intrinsic properties of the materials, and it can be tailored by microstructural engineering (e.g. particle size, porosity, tortuosity, etc.). In this context, different electrode preparation methods have been reported in the literature to obtain nanostructured electrodes with improved properties, such as those based on infiltration, spin-coating and spray-pyrolysis [23–25].

Spray-pyrolysis has been previously used to obtain lanthanum nickelate layers with different morphologies by varying the preparation conditions; however, these materials require temperatures as high as 1000 °C to stabilize the Ruddlesden-Popper structure [26,27]. In contrast, the analogous lanthanum cuprates are single phase compounds at much lower temperatures, minimizing the compatibility problems between the electrolyte and electrode layers [28–31]. In addition, nickel is highly toxic by inhalation, and consequently the preparation of nickel-containing compounds by spray-pyrolysis deposition is not recommendable [32].

In this work, $La_2CuO_{4+\delta}$ (LCO) and $La_{1.7}Sr_{0.3}CuO_{4+\delta}$ (LSCO) cathodes are prepared for the first time by using three different approaches. In the first one, polycrystalline powders are obtained from freeze-dried precursors and then deposited by screen-printing onto a CGO electrolyte (Fig. 1a). In the second and third approaches, the electrodes are prepared in a single deposition step by spray-pyrolysis on as-prepared electrolyte surfaces (Fig. 1b) and onto porous electrolyte backbone layers (Fig. 1c). The latter is an alternative to the traditional wet infiltration technique with several advantages, including shorter preparation time and simplicity of implementation at industrial scale. The structure, microstructure and electrochemical properties of these electrodes are investigated as a function of the sintering temperature.

2. Experimental

2.1. Materials preparation

The $Ce_{0.9}Gd_{0.1}O_{1.95}$ (CGO) electrolyte pellets were prepared by pressing the powders (Rhodia) into disks (10 and 1 mm of diameter and thickness, respectively) and then sintered at 1400 °C for 4 h. Porous backbone layers were formed on the dense pellets by screen-printing a slurry containing CGO powders and Decoflux (Zschimmer and Schwarz), followed by sintering at 1200 °C for 1 h.

In the spray-pyrolysis technique: $La(NO_3)_3 \cdot 6H_2O$, $Cu(NO_3)_2 \cdot 3H_2O$ and $Sr(NO_3)_2$ (Aldrich, purity >99%) were dissolved in distilled water using ethylenediaminetetraacetic acid (EDTA) as chelating agent to obtain the precursor solution of LCO and LSCO.

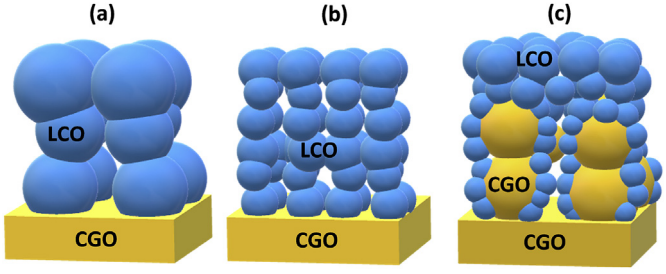

Fig. 1. Microstructural strategies used for the preparation of LCO cathodes: (a) freeze-dried powders, spray-pyrolysis deposition on: (b) as-prepared electrolyte surface (SP) and (c) porous electrolyte backbone (SP-CGO).

Cation and EDTA concentrations were of 0.01 and 0.005 mol L^{-1}, respectively. The spray-pyrolysis procedure was similar to that previously reported for related materials: solution flow rate of 0.02 L h^{-1}, substrate temperature of 350 °C and deposition time of 1 h [33–36]. The deposition was made through a circular shadow mask of 0.25 cm^2 placed symmetrically on both faces of the CGO pellets without and with porous backbone layers. The as-deposited amorphous layers were fired between 600 and 750 °C for 1 h at heating/cooling rates of 2 °C min^{-1} to achieve crystallization.

Polycrystalline powders were also prepared by a freeze-drying precursor method as described elsewhere for similar materials [37]. The corresponding nitrate salts were dissolved in stoichiometric amounts in distilled water with an EDTA:metal molar ratio of 1:1, resulting in a solution with cation concentration and pH of 0.1 mol L^{-1} and 7, respectively. The solutions were frozen in liquid nitrogen and then dehydrated in a Scanvac Coolsafe freeze-dryer for one day. The dried precursors were calcined at 800 °C for 2 h in order to obtain the single-phase compounds. After that, the powders were ball-milled with Decoflux at 250 rpm for 2 h to obtain a slurry, which was screen-printed on both faces of the pellets, and then sintered at different temperatures between 800 and 1000 °C for 2 h.

For simplicity reasons, the different LCO cathode designs are hereafter denoted as FD, SP and SP-CGO for the electrodes obtained from freeze-dried powders (Fig. 1a) and by spray-pyrolysis deposition on the surface of CGO pellets (Fig. 1b) and CGO backbones (Fig. 1c).

2.2. Materials characterization

The composition and structure of the electrodes in form of powders and layers were studied by X-ray powder diffraction (XRD) with an Empyrean PANalytical diffractometer and $CuK\alpha_{1,2}$ radiation. The structural analysis was performed with X'Pert HighScore Plus and GSAS suite softwares [38,39].

Chemical compatibility between LCO and different electrolyte materials, i.e. $Ce_{0.9}Gd_{0.1}O_{1.95}$ (CGO), $Zr_{0.84}Y_{0.16}O_{1.92}$ (YSZ) and $La_{0.9}Sr_{0.1}Ga_{0.8}Mg_{0.2}O_{2.85}$ (LSGM), was reexamined because of the contradictory results reported in the literature [28,40–42]. For this purpose, cathode and electrolyte powders were mixed in a 1:1 wt ratio, fired in a furnace between 800 and 1000 °C for 24 h, and then analyzed by XRD.

The microstructure of the electrodes was observed by electron microscopy, SEM (FEI, Helios Nanolab 650) and TEM (FEI, Talos F200X) equipped with energy dispersive X-ray spectrometer (EDX, X-Max Oxford).

The electrode polarization resistance was determined by impedance spectroscopy (Solartron 1260 FRA) in a symmetrical cell configuration at open circuit voltage (0 V dc bias). The data were collected in static air between 350 and 700 °C, frequency range of 10 mHz - 1 MHz and an AC amplitude of 100 mV. Platinum ink and meshes were used as current collectors. The impedance spectra were also acquired as a function of the oxygen partial pressure to identify the different processes involved in the oxygen reduction reactions [35]. The data were fitted by equivalent circuit models using the ZView software (Scribner Associates).

3. Results and discussion

3.1. Structural analysis

Fig. 2 compares the XRD patterns of $La_2CuO_{4+\delta}$ (LCO) and $La_{1.7}Sr_{0.3}CuO_{4+\delta}$ (LSCO) obtained from freeze-dried powders (FD) and spray-pyrolysis (SP). All materials are single phase compounds after firing between 750 and 800 °C. Below this temperature,

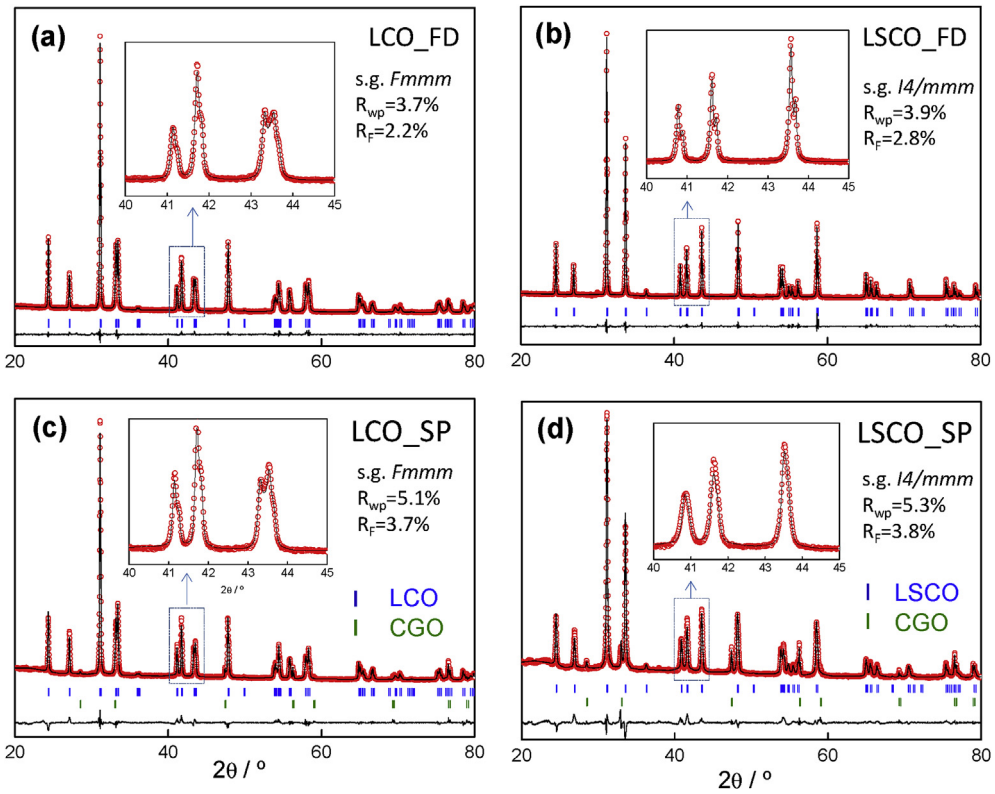

Fig. 2. XRD patterns of $La_2CuO_{4+\delta}$ (LCO) and $La_{1.7}Sr_{0.3}CuO_{4+\delta}$ (LSCO) prepared by (a–b) freeze-dried powders at 800 °C and (c–d) spray-pyrolysis layers at 750 °C.

impurities associated with lanthanum oxide carbonates are observed (Fig. S1, supplementary material). The undoped and Sr-doped compounds crystallize with orthorhombic and tetragonal symmetries, respectively, regardless of the preparation method used.

XRD data for the powder samples have been analyzed by the Rietveld method using the different structural models available in the literature [43–45]. The best fit for LCO is obtained with an orthorhombic *Fmmm* space group with the following agreement factors: $R_{wp} = 3.69\%$ and $R_F = 2.22\%$. Rietveld refinements in other space groups, such as orthorhombic *Bmab*, lead to a worse fitting: $R_{wp} = 4.32\%$ and $R_F = 3.23\%$. The refinement of LSCO is carried out in the tetragonal *I4/mmm* space group, leading also to good agreement factors: $R_{wp} = 3.91\%$ and $R_F = 2.81\%$.

In the case of the layers deposited by spray-pyrolysis onto CGO substrates, two different phases, ascribed to La_2CuO_4 and CGO (s.g. $Fm\bar{3}m$), are considered during the Rietveld refinement. The results are analogous to those obtained for powder samples, with rather similar agreement factors (Fig. 2c and d). Regarding the lattice cell parameters, these are similar for both polycrystalline powders and layers, further confirming that the same materials are obtained by both freeze-drying and spray-pyrolysis methods (Table S1, supplementary information).

The average crystallite size was estimated by using the Scherrer's equation, taking into account the instrumental broadening with LaB_6 as standard reference material. The sizes are approximately of 93 and 75 nm for the freeze-drying and spray-pyrolysis samples, respectively (Table S1, supplementary material).

3.2. Chemical compatibility

Fig. 3 compares the XRD patterns of the electrolyte-cathode powder mixtures after calcining at different temperatures for 24 h. No evidence of reaction is observed at temperatures below 800 °C, indicating appropriate chemical compatibility between the materials at low temperature. These results are further confirmed by the XRD Rietveld analysis, where the unit cell parameters remain very close to those of the pristine materials. Analogous results are observed for LSCO.

Additional diffraction peaks are observed in the YSZ-LCO mixture at 900 °C, which are assigned to $La_2Zr_2O_7$ with a pyrochlore-type structure [41]. As expected, the reaction becomes more important at higher annealing temperatures with 80 wt% of $La_2Zr_2O_7$ at 1000 °C (Fig. 3a).

In the case of the LSGM-LCO mixture (Fig. 3b), additional diffraction peaks are detected at 1000 °C, which have not been identified. However, a noticeable variation of the unit cell volume is observed with respect to pristine material, i.e. the unit cell volume of LCO changes from 95.14 $Å^3$ to 94.64 $Å^3$ after firing the sample at 1000 °C. A similar behavior occurs for the CGO-LCO mixture at the same temperature, where diffraction peaks associated with the formation of a new fluorite-type compound are visible (Fig. 3c). The diffraction peaks of this new phase are shifted to lower 2θ compared to those of the pristine CGO, indicating that it has a larger unit cell volume, i.e. 39.78 and 41.77 $Å^3$ for the pristine and the reaction product materials, respectively. The formation of this reaction product may be explained by La^{3+} diffusion from LCO to CGO, giving rise to a new compound with composition, $(Ce_{0.9}Gd_{0.1})_{1-x}La_xO_{2-\delta}$, and a larger unit cell volume than that of CGO, since the ionic radii of La^{3+} (1.16 Å) is larger than that of Ce^{4+} (0.97 Å) in an 8-fold coordination.

It has to be commented that these results are similar to those reported by Ruíz-Bustos et al. [40]; however, they are contradictory with the findings of Li et al. [31], where no reaction was observed after firing both materials at 1000 °C for 140 h in air. It is also worth noting that the reaction product, $(Ce,Gd, La)O_{2-\delta}$, is an oxide ion

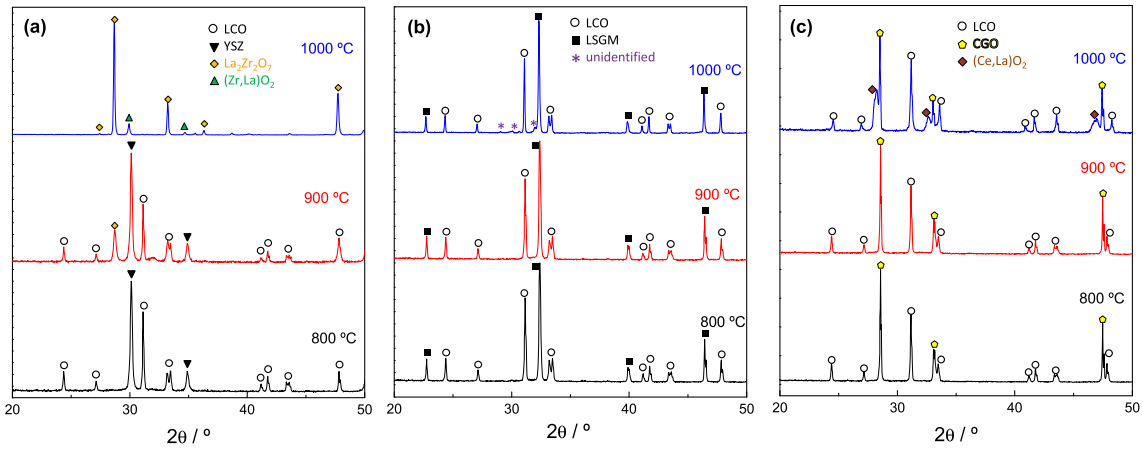

Fig. 3. XRD patterns of (a) YSZ-LCO, (b) LSGM-LCO and (c) CGO-LCO powder mixtures calcined at 800, 900 and 1000 °C for 24 h.

conductor with slightly lower conductivity than CGO, and consequently, the cathode performance is expected not to be seriously affected by the formation of this phase at the electrode/electrolyte interface. In fact, CGO-LSCO composite cathodes showed improved values of polarization resistance when compared to those of the blank cathode, i.e. 0.28 and 0.15 Ω Ω cm^2 for $La_{1.96}Sr_{0.04}CuO_{4+\delta}$ and 20 wt% CGO-$La_{1.96}Sr_{0.04}CuO_{4+\delta}$, respectively at 650 °C [46]. In contrast, the formation of an insulating $La_2Zr_2O_7$ phase at the YSZ/LCO interface blocks the oxygen transport, affecting seriously the cell performance [21,47].

All these results indicate that the fabrication and application of La_2CuO_4-based cathodes should be restricted at temperatures below 800 °C. For this reason, low temperature fabrication methods, such as spray-pyrolysis deposition are needed.

3.3. Microstructure

Fig. 4 shows the cross-section SEM images of the different cathode designs prepared by screen-printing and spray-pyrolysis deposition. As previously commented, the FD powders were sintered at different temperatures in order to investigate the influence of the reactivity on the electrochemical performance. These electrodes have a thickness of approximately 20 μm and exhibit an adequate adherence to the electrolyte, without any visible delamination, at a sintering temperature as low as 800 °C (Fig. 4a). The average grain size is about 330 nm and no evidence of reactivity is observed at the electrode/electrolyte interface (Fig. 4b). The increase of sintering temperature up to 1000 °C leads to a significant coarsening of the microstructure and a grain growth to 800 nm (Fig. 4c). Moreover, nanometric particles, highlighted by arrows in Fig. 4c, are observed at the electrode/electrolyte interface, which are possibly attributed to the reaction product $(Ce,Gd,La)O_{2-\delta}$. The crystallite and particle sizes of the reaction product are about 25 and 35 nm, respectively. It has to be noticed that the cation composition of these particles is not determined by EDX due to the similar composition with the electrolyte.

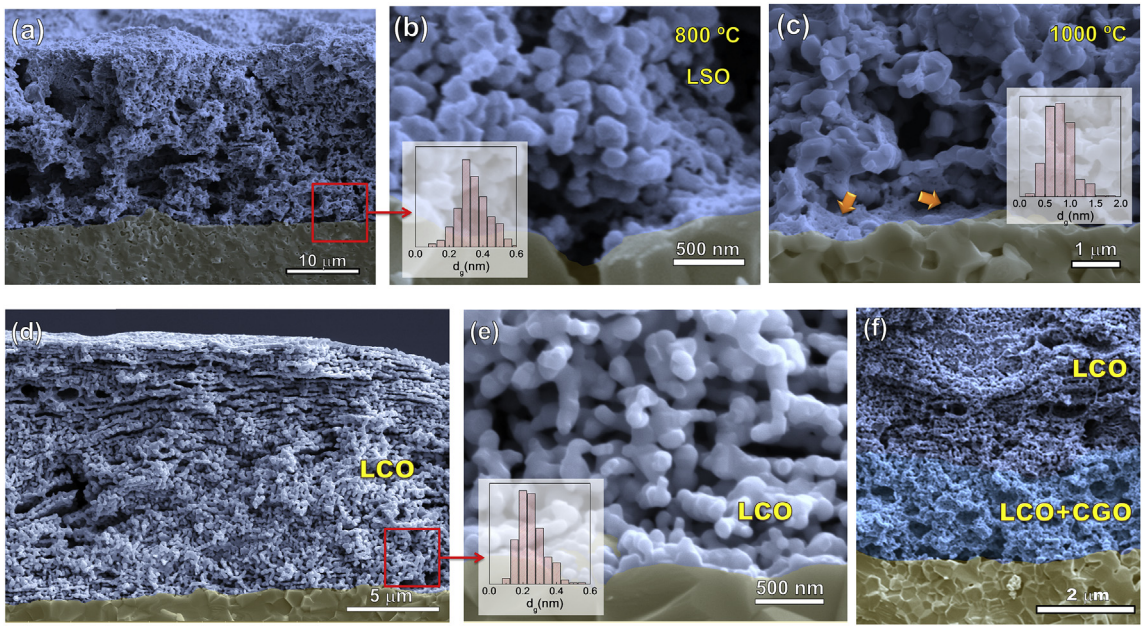

Fig. 4. Cross-sectional SEM image of LCO cathodes prepared by (a) freeze-dried powders and sintered at (b) 800 and (c) 1000 °C for 2 h. (d,e) LCO cathode deposited by spray-pyrolysis at 350 °C and sintered at 750 °C for 1 h. (f) LCO deposited by spray-pyrolysis onto porous CGO backbone.

The same electrodes deposited by spray-pyrolysis at 350 °C and fired at 750 °C exhibit improved microstructural features (Fig. 4d and e). The electrode thickness is comparable to that obtained by screen-printing powders, ~15 μm with uniform and well-connected particles of 220 nm of diameter. In addition, the porosity is more homogeneous when compared to those electrodes obtained by screen-printing. The porosity, estimated from the thickness and mass of the electrodes, takes values of approximately 50 and 40% for the freeze-drying and spray-pyrolysis samples, respectively.

The morphology of LCO cathode deposited on CGO backbone is shown in Fig. 4f. This is comprised of a double layer electrode; where the inner layer is a porous composite of a CGO backbone (2 μm thickness) coated with LCO nanoparticles and, therefore, providing an extended TPB length for the oxygen reduction reactions (Fig. S2, supplementary material). A second layer of LCO particles is formed onto the backbone as a consequence of the excess of material deposited during the spray-pyrolysis process, which is not infiltrated inside the backbone. This layer has a thickness of about 10 μm and exhibits high electrical conductivity compared to the inner CGO-LCO composite layer. Thus, this second layer acts mainly as a current collector and is partially responsible for the enhanced electrochemical properties of this novel electrode architecture.

Scanning transmission electron microscopy-high-angle annular dark-field image (STEM-HAADF) and EDX mapping show a homogeneous distribution of the different elements in LCO samples (Fig. 5a–d). The cation stoichiometry, determined in different points of the cathode layer, is similar to the nominal one within the accuracy limits of the instrument. The materials are highly crystalline after sintering at 750 °C for only 1 h and amorphous phase domains are not detected. Moreover, the interplanar distances are consistent with those determined from XRD data (Fig. 5e).

3.4. Electrochemical characterization

The overall polarization resistance of LCO and LSCO cathodes, prepared from freeze-dried powders, is investigated as a function of the sintering temperature. As can be observed in Fig. S3 (supplementary material), the values of the overall polarization resistance (R_p) for the undoped material (LCO) depend slightly on the sintering temperature, varying from 0.27 to 0.35 Ω cm^2 at a measurement temperature of 700 °C. In contrast, a substantial increase of R_p is observed for Sr-doped compounds (LSCO) as the temperature increases from 800 to 1000 °C, with values of 0.44 and 0.81 Ω cm^2 respectively, at the same measurement temperature of 700 °C. This variation is attributed to two main effects, the microstructure evolution (i.e. grain growth and densification) as the sintering temperature increases, as well as the possible chemical reaction at the electrode-electrolyte interface, as was previously mentioned.

It is also worth noting that LCO, despite having lower electronic conductivity than LSCO (e.g. 20 and 100 S cm^{-1} for LCO and LSCO, respectively [28]), exhibits a lower polarization resistance in the whole temperature range. Thus, the higher R_p variation of LSCO is possibly explained by its stronger reactivity with the CGO electrolyte. These results further demonstrate that the co-sintering temperature of LCO-based materials and CGO should be limited at temperatures as low as possible.

Representative impedance spectra for the different electrode designs are shown in Fig. 6. The spectra are acquired at 600 °C in air atmosphere. It has to be noticed that the electrolyte resistance is subtracted for a better comparison of the electrode response. All the spectra are comprised of two different processes and they are analyzed using the equivalent circuit displayed in the inset of Fig. 6. Two serial resistance-pseudocapacitance (RQ) elements located at low (LF) and high (HF) frequencies are used to model the electrode response. In addition, an inductance (L) and a serial resistance (R_s) are included to consider the electrolyte and the experimental equipment contributions, respectively.

In order to gain further insights on the different contributions involved in the oxygen reduction reaction, the impedance spectra of SP-CGO are collected as a function of the oxygen partial pressure (pO_2) and the different processes are analyzed separately (Fig. 7). The HF contribution possess a capacitance of about 0.5 m Fcm^{-2}

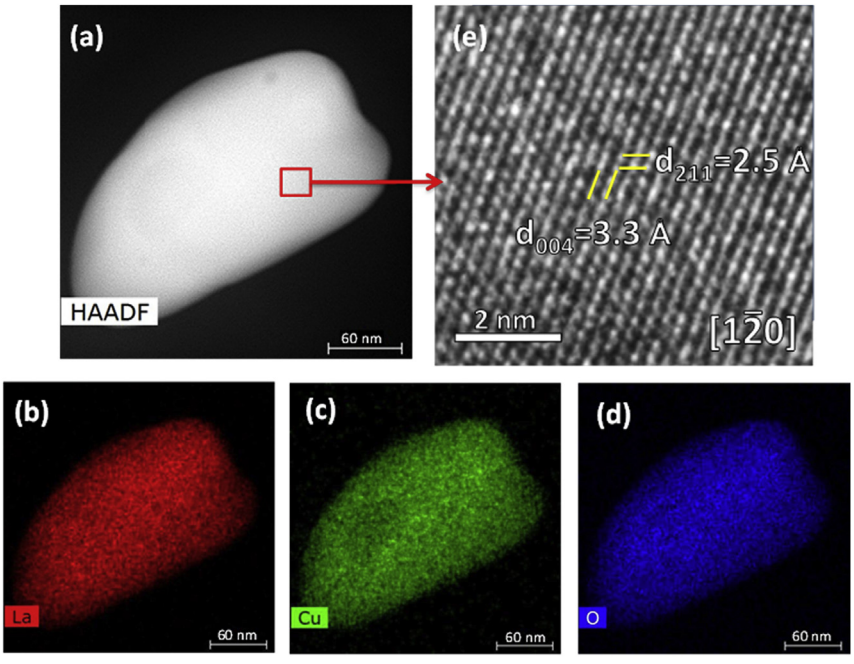

Fig. 5. (a) STEM-HAADF image, (b–d) cation distribution and (e) HR-STEM image of LCO in the [1–20] zone axis.

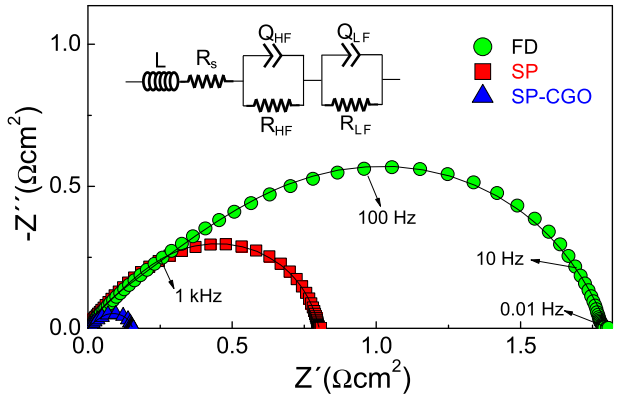

Fig. 6. Representative impedance spectra of LCO cathodes with different microstructural designs at a measured temperature of 600 °C in air atmosphere. The inset figure shows the equivalent circuit model used to fit the data.

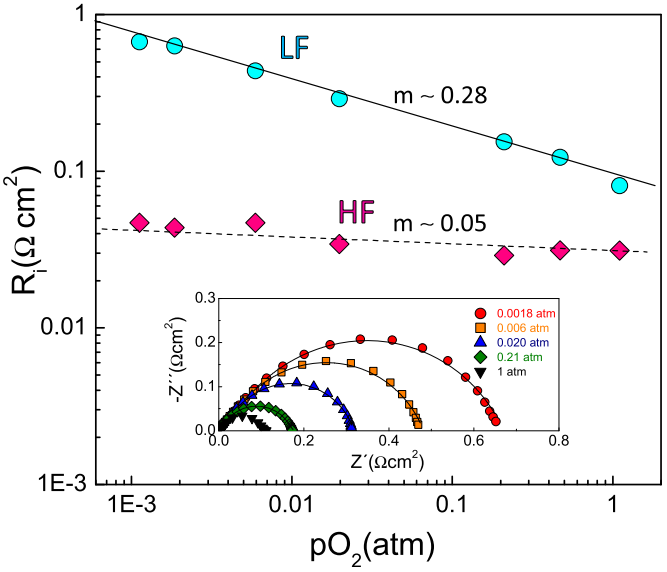

Fig. 7. Variation of the HF and LF contributions to the overall polarization resistance of SP-CGO as a function of the oxygen partial pressure at 600 °C. The inset figure shows the impedance spectra under various pO_2.

and the resistance is nearly pO_2-independent, suggesting that this process is associated with the oxygen ion incorporation from the TPB to the electrolyte ($O^{2-}_{TPB} + V_{\ddot{O}} \rightarrow O^{x}_{o}$). The LF process with a higher capacitance, 10 mF cm^{-2}, shows a ~$(pO_2)^{-1/4}$ dependence, which is assigned to a charge transfer process on the electrode surface ($O_{ads} + 2e^{-} + V_{\ddot{O}} \rightarrow O^{x}_{o}$) [48,49]. It has to be commented that these results are similar to those obtained by Li et al. [28], suggesting that the same processes are involved in micro- and nanostructured cathodes. For all electrode designs, the resistance associated with the LF process is higher than that of the HF process, indicating that change transfer is the rate limiting step to the oxygen reduction reaction (Fig. S4, supplementary material).

The overall polarization resistance of the different LCO designs as a function of the temperature are compared in Fig. 8. The FD electrode exhibits a polarization resistance of 2 Ω cm^2 at 600 °C, which is comparable to those previously reported [28,46]. The SP cathode, deposited on as-prepared CGO electrolyte surfaces, has somewhat lower polarization resistance ~1 Ω cm^2, and this is drastically reduced to 0.14 Ω cm^2 for the SP-CGO cathode deposited by spray-pyrolysis onto a porous CGO backbone. Thus, the

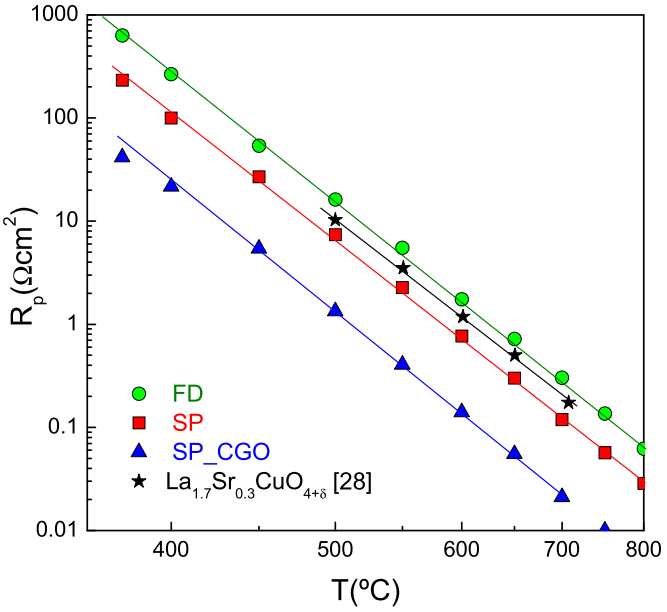

Fig. 8. Temperature variation of the electrode polarization resistance of the different LCO designs. The data of LSCO powder cathodes extracted from the literature [28] are included for comparison purpose.

polarization resistance of SP-CGO is reduced by a factor of 14 compared to FD. This improvement is clearly attributed to the novel architecture of this electrode with a larger contact area between the ionic conductor CGO and the mixed conductor LCO, and consequently, a larger TPB length for the oxygen reduction reactions. Moreover, the porous CGO backbone provides an ionic conducting pathway between the electrode and the electrolyte, improving the oxygen incorporation from TPB to the electrolyte. Finally, the top LCO layer, with a higher electronic conductivity, achieves a homogeneous current distribution within the CGO-LCO composite electrode, leading to further enhancement of the electrical performance. On the other hand, it has to be commented that the polarization resistance results of LSCO are similar to those obtained for the undoped LCO, and for this reason they are not included in Fig. 8.

It is also worth noting that the values of R_p are lower than those previously reported in the literature for lanthanum cuprates, i.e. 1 Ω cm^2 for LSCO [28] and 0.75 Ω cm^2 for CGO-LSCO composite cathode [46] at 600 °C, and they are even lower than the best value reported previously in the literature for lanthanum nickelates obtained by electrostatic spray deposition, i.e. 0.21 Ω cm^2 at 600 °C [27]. Finally, a short-term stability test (~100 h) shows a negligible degradation of both the polarization and serial resistances of SP-CGO cells at 650 °C (Fig. S5, supplementary material).

In summary, spray-pyrolysis is a simple and economic method to obtain high efficiency $La_2CuO_{4+\delta}$ cathodes for SOFCs. The low fabrication temperature, used in the present work, minimizes the reaction between LCO and CGO electrolyte. In addition, the optimized microstructural design of SP-CGO leads to significantly lower values of polarization resistance.

4. Conclusions

$La_2CuO_{4+\delta}$ and $La_{1.7}Sr_{0.3}CuO_{4+\delta}$ cathode materials with different microstructural architectures have been prepared by screen-printing of freeze-dried powders, and by spray-pyrolysis deposition on CGO pellets without and with porous CGO backbones. XRD analysis showed that $La_2CuO_{4+\delta}$ and $La_{1.7}Sr_{0.3}CuO_{4+\delta}$ crystallize in

orthorhombic and tetragonal structures, respectively, regardless of the preparation method. Compatibility studies of lanthanum cuprates with different electrolytes (YSZ, LSGM and CGO) demonstrated reactivity between the materials at sintering temperatures higher than 800 °C, limiting the fabrication and application of these cathodes at the low temperature range.

The electrodes prepared by spray-pyrolysis at lower sintering temperatures showed improved microstructural features, such as smaller grain size and uniform porosity. In addition, the cathode prepared by spray-pyrolysis onto a CGO backbone exhibited the lowest values of polarization resistance, i.e. 0.14 Ω cm^2 compared to 2 Ω cm^2 for FD at 600 °C, which is related to the optimized microstructural architecture of these electrodes.

Acknowledgements

This work has been supported by MINECO (Ministerio de Economía y Competitividad) though the MAT2016-77648-R and EC2014-53906-R research grants (Spain), which is cofounded by FEDER. L. dos Santos-Gómez and J.M. Porras-Vázquez thank to the University of Malaga for the funding.

Appendix A. Supplementary data

Supplementary data to this article can be found online at https://doi.org/10.1016/j.jallcom.2019.02.237.

References

[1] M.G. Turgut, Review of electrical energy storage technologies, materials and systems: challenges and prospects for large-scale grid storage, Energy Environ. Sci. 11 (2018) 2696–2767.
[2] U.M. Damo, M.L. Ferrari, A. Turan, A.F. Massardo, Solid oxide fuel cell hybrid system: a detailed review of an environmentally clean and efficient source of energy, Energy 168 (2019) 235–246.
[3] Z. Gao, L.V. Mogni, E.C. Miller, J.G. Railsback, S.A. Barnett, A perspective on low-temperature solid oxide fuel cells, Energy Environ. Sci. 9 (2016) 1602–1644.
[4] Y. Zhang, R. Knibbe, J. Sunarso, Y. Zhong, W. Zhou, Z. Shao, Z. Zhu, Recent progress on advanced materials for solid-oxide fuel cells operating below 500 °C, Adv. Mater. 29 (2017), 1700132.
[5] Y. Li, W. Zhang, Y. Zheng, J. Chen, B. Yu, Y. Chen, M. Liu, Controlling cation segregation in perovskite-based electrodes for high electro-catalytic activity and durability, Chem. Soc. Rev. 46 (2017) 6345–6378.
[6] F.S. da Silva, T.M. de Souza, Novel materials for solid oxide fuel cell technologies: a literature review, Int. J. Hydrogen Energy 42 (41) (2017) 26020–26036.
[7] A. Orera, P.R. Slater, New chemical systems for solid oxide fuel cells, Chem. Mater. 22 (2010) 675–690.
[8] A. Jun, J. Kim, J. Shin, G. Kim, Perovskite as a cathode material: a review of its role in solid-oxide fuel cell technology, ChemElectroChem 3 (2016) 511–530.
[9] Z. Shao, S.M. Haile, A high-performance cathode for the next generation of solid-oxide fuel cells, Nature 431 (2004) 170–173.
[10] A. Tarancón, S.J. Skinner, R.J. Chater, F. Hernández-Ramírez, J.A. Kilner, Layered perovskites as promising cathodes for intermediate temperature solid oxide fuel cells, J. Mater. Chem. 17 (2007) 3175–3181.
[11] L. Zhang, J. Shan, Q. Wang, $BaCo_{0.4}Fe_{0.4}Zr_{0.2}O_{3-\delta}$: evaluation as a cathode for ceria-based electrolyte IT-SOFCs, J. Alloys Compd. 771 (2019) 221–227.
[12] A. Jun, J. Kim, J. Shin, G. Kim, Perovskite as a cathode material: a review of its role in solid-oxide fuel cell technology, ChemElectroChem 3 (4) (2016) 511–530.
[13] A.A. Yaremchenko, M.V. Patrakeev, E.N. Naumovich, D.D. Khalyavin, The $p(O_2)$-T stability domain of cubic perovskite $Ba_{0.5}Sr_{0.5}Co_{0.8}Fe_{0.2}O_{3-\delta}$, Phys. Chem. Chem. Phys. 20 (6) (2018) 4442–4454.
[14] B. Sikder, A. Chanda, Mechanical characterization of BSCF, a prospective perovskite material for oxygen separation membrane: a brief review, Adv. Eng. Mater. 18 (9) (2016) 1529–1536.
[15] S.J. Skinner, J.A. Kilner, Oxygen diffusion and surface exchange in $La_{2-x}Sr_xNiO_{4+\delta}$, Solid State Ionics 135 (2000) 709–712.
[16] E. Boehm, J.M. Bassat, P. Dordor, F. Mauvy, J.C. Grenier, Ph. Stevens, Oxygen diffusion and transport properties in non-stoichiometric $Ln_{2-x}NiO_{4+\delta}$ oxides, Solid State Ionics 176 (2005) 2717–2725.
[17] N.A. Baharuddin, A. Muchtar, M.R. Somalu, Short review on cobalt-free cathodes for solid oxide fuel cells, Int. J. Hydrogen Energy 42 (2017) 9149–9155.
[18] M. Benamira, A. Ringuedé, M. Cassir, D. Horwat, P. Lenormand, F. Ansart, J.M. Bassat, J.P. Viricelle, Enhancing oxygen reduction reaction of YSZ/$La_2NiO_{4+\delta}$ using an ultrathin $La_2NiO_{4+\delta}$ interfacial layer, J. Alloys Compd. 746 (2018) 413–420.
[19] R. Sayers, J. Liu, B. Rustumji, S.J. Skinner, Novel K_2NiF_4-type materials for solid oxide fuel cells: compatibility with electrolytes in the intermediate temperature range, Fuel Cell 8 (2008) 338–343.
[20] A. Montenegro-Hernández, A. Soldati, L. Mogni, H. Troiani, A. Schreiber, F. Soldera, A. Caneiro, Reactivity at the $Ln_2NiO_{4+\delta}$/electrolyte interface (Ln=La, Nd) studied by electrochemical impedance spectroscopy and transmission electron microscopy, J. Power Sources 265 (2014) 6–13.
[21] A. Montenegro-Hernández, L. Mogni, A. Caneiro, $La_2NiO_{4+\delta}$ as cathode for SOFC: reactivity study with YSZ and CGO electrolytes, Int. J. Hydrogen Energy 35 (2010) 6031–6036.
[22] D. Cetin, S. Poizeau, J. Pietras, S. Gopalan, Decomposition of La_2NiO_4 in $Sm_{0.2}Ce_{0.8}O_2$-La_2NiO_4 composites for solid oxide fuel cell applications, Solid State Ionics 300 (2017) 91–96.
[23] J.M. Vohs, R.J. Gorte, High-performance SOFC cathodes prepared by infiltration, Adv. Mater. 21 (2009) 943–956.
[24] D. Chen, C. Chen, Z.M. Baiyee, Z. Shao, F. Ciucci, Nonstoichiometric oxides as low-cost and highly-efficient oxygen reduction/evolution catalysts for low-temperature electrochemical devices, Chem. Rev. 115 (2015) 9869–9921.
[25] A.M. Abdalla, S. Hossain, A.T. Azad, P.M.I. Petra, F. Begum, S.G. Eriksson, A.K. Azad, Nanomaterials for solid oxide fuel cells: a review, Renew. Sustain. Energy Rev. 82 (2018) 353–368.
[26] T. Ryll, P. Reibisch, L. Schlagenhauf, A. Bieberle-Huetter, M. Döbeli, J.L.M. Rupp, L.J. Gauckler, Lanthanum nickelate thin films deposited by spray pyrolysis: crystallization, microstructure and electrochemical properties, J. Eur. Ceram. Soc. 32 (2012) 1701–1709.
[27] R.K. Sharma, E. Djurado, Functionally graded and homogeneous composites of $La_2NiO_{4+\delta}$ and $La_{n+1}Ni_nO_{3n+1}$ (n = 2 and 3) solid oxide fuel cell cathodes, J. Mater. Chem. A 5 (2017) 22277–22287.
[28] Q. Li, H. Zhao, L. Huo, L. Sun, X. Cheng, J.C. Grenier, Electrode properties of Sr doped La_2CuO_4 as new cathode material for intermediate-temperature SOFCs, Electrochem. Commun. 9 (2007) 1508–1512.
[29] K. Zheng, A. Gorzkowska-Sobaś, K. Świerczek, Evaluation of Ln_2CuO_4 (Ln: La, Pr, Nd) oxides as cathode materials for IT-SOFCs, Mater. Res. Bull. 47 (2012) 4089–4095.
[30] M.S. Kaluzhskikh, S.M. Kazakov, G.N. Mazo, S.Y. Istomin, E.V. Antipov, A.A. Gippius, Y. Fedotov, S.I. Bredikhin, Y. Liu, G. Svensson, Z. Shen, High-temperature crystal structure and transport properties of the layered cuprates Ln_2CuO_4, Ln=Pr, Nd and Sm, J. Solid State Chem. 184 (2011) 698–704.
[31] Z. Zhang, Z. Du, A. Niemczyk, K. Li, H. Zhao, K. Świerczek, A-site non-stoichiometry and B-site doping with selected M^{3+} cations in $La_{2-x}Cu_{1-y-z}Ni_yM_zO_{4-\delta}$ layered oxides, Solid State Ionics 317 (2018) 26–31.
[32] D. Schaumlöffel, Nickel species: analysis and toxic effects, J. Trace Elem. Med. Biol. 26 (2012) 1–6.
[33] D. Marrero-López, L. dos Santos-Gómez, J. Canales-Vázquez, F. Martín, J.R. Ramos-Barrado, Stability and performance of nanostructured $La_{0.8}Sr_{0.2}MnO_{3-\delta}$ cathodes deposited by spray-pyrolysis, Electrochim. Acta 134 (2014) 159–166.
[34] L. dos Santos-Gómez, E.R. Losilla, F. Martín, J.R. Ramos-Barrado, D. Marrero-López, Novel microstructural strategies to enhance the electrochemical performance of $La_{0.8}Sr_{0.2}MnO_{3-\delta}$ cathodes, ACS Appl. Mater. Interfaces 7 (2015) 7197–7205.
[35] D. Marrero-López, R. Romero, F. Martín, J.R. Ramos-Barrado, Effect of the deposition temperature on the electrochemical properties of $La_{0.6}Sr_{0.4}Co_{0.8}Fe_{0.2}O_{3-\delta}$ cathode prepared by conventional spray-pyrolysis, J. Power Sources 255 (2014) 308–317.
[36] L. dos Santos-Gómez, J.M. Porras-Vázquez, E.R. Losilla, D. Marrero-López, Improving the efficiency of layered perovskite cathodes by microstructural optimization, J. Mater. Chem. A 5 (2017) 7896–7904.
[37] A.J. Fernández-Ropero, J.M. Porras-Vázquez, A. Cabeza, P.R. Slater, D. Marrero-López, E.R. Losilla, High valence transition metal doped strontium ferrites for electrode materials in symmetrical SOFCs, J. Power Sources 249 (2014) 405–413.
[38] X'Pert, HighScore Plus, version 3.0e, PANalytical BV. Amelo, The Netherlands, 2018.
[39] A.C. Larson, R.B. von Dreele, GSAS Program, Los Alamos National Lab, 1994. Rep. No. LA-UR-86748.
[40] R. Ruíz-Bustos, A. Cantos-Gómez, A.J. Dos Santos-García, C. Sánchez-Bautista, J. Van Duijn, On the stability of Sr-doped La_2CuO_4 against different electrolytes for IT-SOFCs, Fuel Cells 11 (2011) 59–64.
[41] H.C. Yu, K.Z. Fung, Reaction between strontium-doped lanthanum cuprate and yittria-stabilized zirconia, J. Am. Ceram. Soc. 89 (2006) 2881–2886.
[42] D. Pérez-Coll, A. Aguadero, M.J. Escudero, P. Núñez, L. Daza, Optimization of the interface polarization of the La_2NiO_4-based cathode working with the $Ce_{1-x}Sm_xO_{2-\delta}$ electrolyte system, J. Power Sources 178 (2008) 151–162.
[43] Inorganic Crystal Structure Database (ICSD) 2018. v2018-01.
[44] P.G. Radaelli, D.G. Hinks, A.W. Mitchell, B.A. Hunter, J.L. Wagner, B. Dabrowski, K.G. Vandervoort, H.K. Viswanathan, J.D. Jorgensen, Structural and superconducting properties of $La_{2-x}Sr_xCuO_4$ as a function of Sr content, Phys. Rev. B 49 (1994) 4163–4175.
[45] R.M. Fleming, B. Batlogg, R.J. Cava, E.A. Rietman, Temperature and composition dependence of the tetragonal-orthorhombic distortion in $La_{2-x}Sr_xCuO_{4-\delta}$, Phys. Rev. B 35 (1987) 7191–7194.
[46] S.J. Lee, P. Muralidharan, S.H. Jo, D.K. Kim, Composite cathode for IT-SOFC: Sr-

doped lanthanum cuprate and Gd-doped ceria, Electrochem. Commun. 12 (2010) 808–811.
[47] Y. Chen, L. Yang, F. Ren, K. An, Visualizing the structural evolution of LSM/xYSZ composite cathodes for SOFC by in-situ neutron diffraction, Sci. Rep. 4 (2014) 5179.
[48] Y. Takeda, R. Kanno, M. Noda, Y. Tomida, O. Yamamoto, Cathodic polarization phenomena of perovskite oxide electrodes with stabilized zirconia, J. Electrochem. Soc. 134 (1987) 2656–2661.
[49] M.J. Escudero, A. Aguadero, J.A. Alonso, L. Daza, A kinetic study of oxygen reduction reaction on La_2NiO_4 cathodes by means of impedance spectroscopy, J. Electroanal. Chem. 611 (2007) 107–116.